IMPORTANCE SAMPLING FOR MULTI-NEGATIVE MULTIMODAL DIRECT PREFERENCE OPTIMIZATION

Anonymous authors
Paper under double-blind review

ABSTRACT

Direct Preference Optimization (DPO) has recently been extended from text-only models to vision-language models. However, existing methods rely on oversimplified pairwise comparisons, generating a single negative image via basic perturbations or similarity-based retrieval, which fail to capture the complex nature of multimodal preferences, inducing optimization bias and hallucinations. To address this issue, we propose MISP-DPO, the first framework to incorporate *multiple*, semantically *diverse* negative images in multimodal DPO via the Plackett-Luce model. Our method embeds prompts and candidate images in CLIP (Contrastive Language–Image Pre-training) space and applies a sparse autoencoder to uncover semantic deviations into interpretable factors. Negative samples are selected based on reconstruction difficulty, semantic deviation from the positive, and mutual diversity, yielding broader and more informative supervision. To handle multi-negative comparisons, we adopt a Plackett–Luce objective and introduce an importance sampling strategy that improves training efficiency. Experiments across five diverse benchmarks demonstrate that MISP-DPO consistently improves multimodal alignment over prior methods, validating the effectiveness of semantic-aware, multi-negative sampling in preference-based learning.

1 INTRODUCTION

Direct Preference Optimization (DPO) (Rafailov et al., 2023; Amini et al., 2024) has shown great promise for aligning language models by learning from pairwise comparisons, bypassing the need for explicit reward modeling. Recent efforts have extended DPO to multimodal contexts, enhancing vision-language model (VLM) alignment through image-text feedback(Wang et al., 2024a; Jiang et al., 2024; Deng et al., 2024; Fu et al., 2025; Liu et al., 2025; Wu et al., 2025; Xing et al., 2025). However, simply extending textual preference data to multimodal scenarios often introduces new challenges, particularly exacerbating hallucinations (Wang et al., 2024a; Fu et al., 2025; Wu et al., 2025). Existing multimodal DPO methods generate only a single negative image per comparison, typically via adversarial cropping, random perturbations, or similarity-based retrieval (Liu et al., 2025; Fu et al., 2025; Wu et al., 2025; Xing et al., 2025). This oversimplifies the rich space of visual negatives, reducing supervision to a single dimension and limiting the model's ability to generalize. For instance, as illustrated in Figure 1, avoiding a single negative depicting a "green apple" might teach the model to reject green hues but ignore mismatched contexts like "kitchen counter" or incorrect objects like "pear." By optimizing against narrow, one-dimensional deviations, models risk spurious correlations, bias amplification, and persistent hallucinations.

The core challenge is that images lack explicit, compositional units like text tokens, making it difficult to isolate meaningful visual deviations (Sahin et al., 2024; Zeng et al., 2024; Zheng et al., 2024; Hsieh et al., 2023; Kamath et al., 2024; 2023). Naive perturbations often destroy overall coherence without isolating meaningful deviations, making it difficult to systematically explore the negative factors of model weaknesses. Effective learning requires disentangling and surfacing multiple latent error factors while maintaining prompt relevance. Existing methods incorporate these factors into a single negative example, leaving models blind to orthogonal error types.

To address this, we propose MISP-DPO, the first framework to introduce *multi*-negative, semantically *diverse* supervision into multimodal DPO. Our approach consists of two stages,

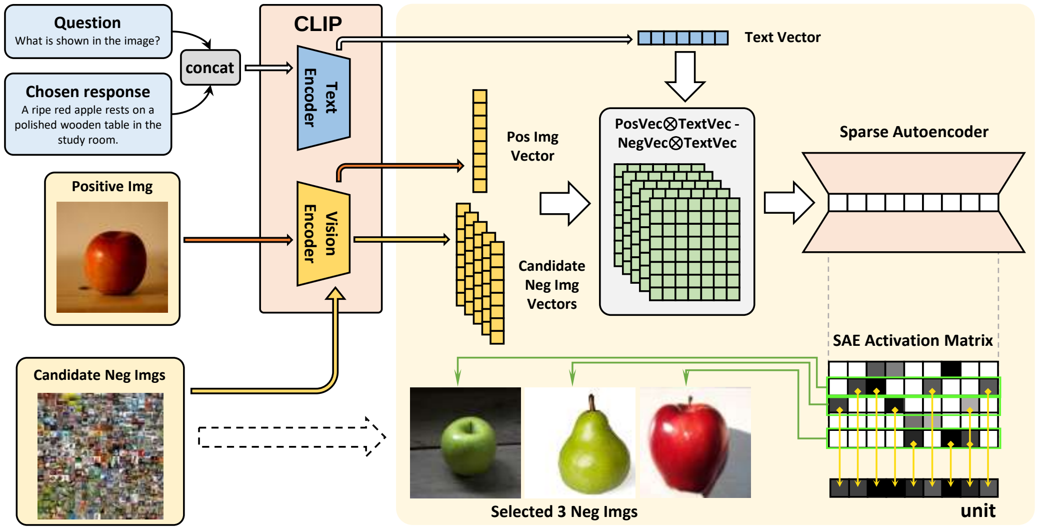

Figure 1: Overview of the MISP-DPO framework, which integrates CLIP encoding and sparse autoencoder–guided selection to identify diverse negatives for multi-negative preference optimization.

- In the first stage, we select diverse image-side negatives from a large open-domain pool. Prompts and candidate images are embedded in CLIP (Radford et al., 2021) space, and a sparse autoencoder (SAE) decomposes their semantic differences into disentangled latent factors (e.g., object, color, layout). We prioritize negatives based on: (1) reconstruction error (informativeness), (2) semantic deviation from the positive sample, and (3) mutual diversity, ensuring broad coverage of negative types.
- In the second stage, we integrate these multiple negatives into a generalized DPO objective using the Plackett–Luce model. Rather than relying on binary comparisons, our approach ranks a positive image above a diverse set of negatives, forcing the model to resolve multiple constraints simultaneously. We further introduce an importance sampling scheme guided by SAE-derived scores, improving training efficiency.

We evaluate MISP-DPO on five multimodal benchmarks (Sun et al., 2023; Guan et al., 2024; Lu et al., 2024; Tong et al., 2024; Li et al., 2023a) focused on hallucination reduction and visual grounding. Our method consistently outperforms strong baselines, achieving notable hallucination reduction and improved alignment, including a 30.09% average improvement over LLaVA-v1.5-7B (Liu et al., 2023).

Our contributions are as follows:

- We propose the first framework to incorporate multi-negative supervision into multimodal DPO, leveraging semantic diversity to systematically reduce hallucinations.
- We introduce an efficient negative sampling method based on CLIP embeddings and SAE–guided importance sampling, providing semantically informative negative examples.
- Extensive evaluations demonstrate that our method substantially reduces hallucinations and achieves robust multimodal alignment across multiple benchmarks.

2 RELATED WORKS

Multimodal Direct Preference Optimization. DPO (Rafailov et al., 2023) has become a widely adopted method for aligning LLMs with human preferences due to its simplicity and stability. However, when extended to multimodal scenarios, especially for hallucination-prone tasks, standard DPO often fails to effectively incorporate visual signals, leading models to overfit textual biases and ignore image-grounded constraints. To mitigate this, recent works have adapted DPO for multimodal hallucination reduction by incorporating visual preference supervision. mDPO (Wang et al., 2024a) introduces conditional preference learning and reward anchoring, using lightweight perturbations (e.g., cropping, diffusion) to construct visual negatives. CHiP (Fu et al., 2025) further complements this with hierarchical textual supervision and a visual contrastive loss to better align fine-grained text and image semantics. While both methods demonstrate notable gains on hallucination benchmarks, they rely on limited forms of visual augmentation, often constrained to local perturbations with narrow semantic variation. Other approaches, such as S-VCO (Wu et al., 2025) and Re-Align (Xing et al., 2025), explore counterfactual or retrieval-based visual negative generation, but at the cost of high computation and limited scalability. In this work, we follow the hallucination-centric preference optimization paradigm initiated by mDPO, and propose a scalable framework for generating informative visual negatives tailored for multimodal preference learning.

Multi-negative Preference Optimization. Recent works in textual and recommendation domains (Amini et al., 2024; Shi et al., 2024; Baruch et al.) have extended DPO to multi-negative settings, ranking positives above multiple negatives to enhance robustness. For example, Softmax-DPO (Chen et al., 2024a) and DMPO (Shi et al., 2024) adopt soft ranking or Plackett–Luce objectives to reduce noise sensitivity. However, such techniques remain underexplored in vision-language models, where negatives must capture subtle cross-modal semantic shifts. Inspired by findings in attribute-based recognition (Yan et al., 2023; Wang et al., 2024b) showing that compact, curated subsets can match large noisy sets, we adapt this insight to multimodal preference learning. Our framework uses a sparse autoencoder in CLIP space to select semantically diverse negatives, enabling importance-weighted ranking over multiple contrastive examples and capturing fine-grained failure modes more effectively.

3 PRELIMINARIES

3.1 MULTIMODAL DIRECT PREFERENCE OPTIMIZATION

DPO (Rafailov et al., 2023) provides a principled way to align a learned policy with human preference judgments without explicitly modeling rewards. In the RLHF framework, solving for the optimal policy π^* under a fixed reference policy π_{ref} yields a latent reward function

$$r(x, y) = \beta \log \frac{\pi^*(y \mid x)}{\pi_{\text{ref}}(y \mid x)} + Z(x), \tag{1}$$

where β scales the strength of alignment and $Z(x)$ is a prompt-dependent normalizer. Substituting this into the Bradley–Terry–Luce model and dropping $Z(x)$ gives a simple training objective for a parametric policy π_θ,

$$\mathcal{L}_{\text{DPO}}(\theta) = -\mathbb{E}_{(x,y_p,y_n)\sim D}\Big[\log \sigma\big(\beta \log \tfrac{\pi_\theta(y_p|x)}{\pi_{\text{ref}}(y_p|x)} \;-\; \beta \log \tfrac{\pi_\theta(y_n|x)}{\pi_{\text{ref}}(y_n|x)}\big)\Big]. \tag{2}$$

Recent work extends DPO to vision-language models (VLMs) by incorporating visual preferences. Let x denote the multimodal prompt, m_p a preferred image aligned with textual response y_p, and m_n a rejected image. The multimodal reward $r(m, x, y)$ now depends on visual grounding, with preferences modeled as,

$$p^*(y_p \succ y_n \mid m, x) = \sigma\big(r(m, x, y_p) - r(m, x, y_n)\big).$$

To ensure a fair comparison across images, we hold y_p fixed and vary only the image input, the multimodal DPO loss (Wang et al., 2024a; Fu et al., 2025; Wu et al., 2025) focuses on visual discrimination,

$$\mathcal{L}_{\text{DPO}_{\text{img}}}(\theta) = -\mathbb{E}_{(m_p,m_n,x,y_p)\sim D}\Big[\log \sigma\big(\beta \log \tfrac{\pi_\theta(y_p|m_p,x)}{\pi_{\text{ref}}(y_p|m_p,x)} - \beta \log \tfrac{\pi_\theta(y_p|m_n,x)}{\pi_{\text{ref}}(y_p|m_n,x)}\big)\Big]. \tag{3}$$

This formulation supports joint optimization over visual and textual inputs, enabling the policy to associate preferred images with relevant multimodal features.

3.2 MULTI-NEGATIVE PREFERENCE OPTIMIZATION

Multi-negative preference optimization (Chen et al., 2024a) extends the Direct Preference Optimization approach (Rafailov et al., 2023), enabling language models to be trained against several negative preferences rather than just one. Instead of using the Bradley–Terry formulation for single pairwise comparisons, this method adopts the Plackett–Luce model (Plackett, 1975; Luce et al., 1959) to score a target choice in relation to an entire set of inferior alternatives.

Given a prompt x, a preferred response y_p, and a set of N non-preferred responses $\mathcal{Y}_n = \{y_n^i\}_{i=1}^N$, the Plackett–Luce probability that y_p is ranked above all y_n^i is

$$p^*(y_p \succ \mathcal{Y}_n \mid x) = \frac{\exp\bigl(r(x, y_p)\bigr)}{\exp\bigl(r(x, y_p)\bigr) \; + \; \sum_{i=1}^N \exp\bigl(r(x, y_n^i)\bigr)}, \tag{4}$$

where $r(x, y)$ is the latent reward function. Substituting

$$r(x, y) = \beta \, \log \frac{\pi_\theta(y \mid x)}{\pi_{\mathrm{ref}}(y \mid x)} \; + \; Z(x)$$

and noting that $Z(x)$ cancels in the ratio gives

$$p^*(y_p \succ \mathcal{Y}_n \mid x) = \frac{1}{1 + \sum_{i=1}^N \exp\bigl(\beta \, \Delta_i\bigr)}, \quad \Delta_i = \log \frac{\pi_\theta(y_n^i \mid x)}{\pi_{\mathrm{ref}}(y_n^i \mid x)} - \log \frac{\pi_\theta(y_p \mid x)}{\pi_{\mathrm{ref}}(y_p \mid x)}.$$

Hence the multi-negative DPO training objective becomes

$$\mathcal{L}_{\text{MN-DPO}}(\theta) = -\,\mathbb{E}_{(x, y_p, \mathcal{Y}_n) \sim D}\Bigl[\log \sigma\bigl(-\,\log \sum_{i=1}^N \exp\bigl(\beta \, \Delta_i\bigr)\bigr)\Bigr]. \tag{5}$$

Notably, when $N = 1$, $\mathcal{L}_{\text{MN-DPO}}$ in equation 5 reduces exactly to the single-negative DPO loss.

4 FRAMEWORK

We propose MISP-DPO, a framework that address the limitations of single-negative supervision by introducing multi-negative learning through two core components: (1) a diverse negative sampling strategy using sparse autoencoders to identify semantically meaningful deviations, and (2) a generalized Plackett-Luce ranking objective that integrates multiple negatives to promote robust alignment. An overview of the framework is shown in Figure 1.

4.1 MULTI-NEGATIVE OBJECTIVES

Due to the limitations of single-negative supervision and the inherently multi-faceted nature of visual errors, we extend multimodal DPO to a multi-negative preference optimization setting. Let π_θ denote the VLM policy to be optimized. Each training instance consists of a multimodal prompt x, a preferred image m_p paired with an aligned textual response y_p, and a set of N negative images $S_n = \{m_n^i\}_{i=1}^N$ from open-domain sources. Following the Plackett-Luce formulation from Eq. equation 4, we adapt equation 5 to visual preferences,

$$\mathcal{L}_{\mathrm{img}}(\theta; S_n) = \log \sigma \left(-\log \sum_{i \in S_n} \exp \left(\beta \log \frac{\pi_\theta(y_p \mid x, m_n^i)}{\pi_{\mathrm{ref}}(y_p \mid x, m_n^i)} - \beta \log \frac{\pi_\theta(y_p \mid x, m_p)}{\pi_{\mathrm{ref}}(y_p \mid x, m_p)} \right) \right) \tag{6}$$

This extends Eq. equation 3 to multiple negatives through the softmax aggregation and encourages the model to assign higher preference scores to the correct image m_p compared to all negative images in S_n, thereby promoting more robust visual grounding.

Lemma 4.1 (Gradient Decomposition) *Defining the preference advantage of each negative image and the preference distribution as*

$$a_i = \beta \left(\log \frac{\pi_\theta(y_p \mid x, m_n^i)}{\pi_{\mathrm{ref}}(y_p \mid x, m_n^i)} - \log \frac{\pi_\theta(y_p \mid x, m_p)}{\pi_{\mathrm{ref}}(y_p \mid x, m_p)} \right), \quad p_\theta(m_n^i \mid x, m_p, y_p) = \frac{\exp(a_i)}{\sum_{j=1}^N \exp(a_j)}.$$

Then the gradient of equation 6 decomposes as,

$$\nabla_\theta \mathcal{L}_{\mathrm{img}}(\theta; \mathcal{S}_n) = \beta \sigma\Bigl(\log \sum_{i=1}^N \exp(a_i)\Bigr) \sum_{i=1}^N p_\theta(m_n^i \mid x, m_p, y_p) \Delta_\theta(m_n^i, m_p \mid x, y_p), \tag{7}$$

where $\Delta_\theta(m_n^i, m_p \mid x, y_p) = \nabla_\theta \log \pi_\theta(y_p \mid x, m_n^i) - \nabla_\theta \log \pi_\theta(y_p \mid x, m_p)$.

This result shows that the gradient is a weighted combination of correction signals across the image space, offering interpretability in terms of how the model adjusts its predictions in response to each visual discrepancy.

Although Eq.(6) and its gradient give an unbiased update, they require drawing a large set of negatives from the true $p_\theta(m_n^i \mid x, m_p, y_p)$ and computing $S(\{m_n^i\})$. In realistic image domains, neither step is tractable. To alleviate this, we introduce a learnable distribution $q_\phi(m_n \mid x, m_p, y_p)$ to sample a small candidate pool $\tilde{S}_n$. Rewriting the gradient illustrated in Lemma 4.1 as an expectation under q_ϕ gives a *importance-sampling* estimator,

$$\nabla_\theta \mathcal{L}_{\text{img}}(\theta; \tilde{S}_n) = \beta\sigma\Big(\log \sum_{i\in\tilde{S}_n} \exp(a_i)\Big) \sum_{i\in\tilde{S}_n} \frac{\exp(a_i)}{q_\phi(m_n^i \mid x, m_p, y_p)} \Delta_\theta(m_n^i, m_p \mid x, y_p). \quad (8)$$

To encourage joint reasoning across modalities, we extend our framework by incorporating textual preference supervision. We follow recent multimodal DPO methods and replace traditional text-only preferences with image-grounded negative responses y_n for the same prompt and image m_p. The corresponding DPO loss is,

$$\mathcal{L}_{\text{text}}(\theta; \tilde{\mathcal{S}}_n) = \log\sigma\Big(\beta \log \frac{\pi_\theta(y_p \mid x, m_p)}{\pi_{\text{ref}}(y_p \mid x, m_p)} - \beta \log \frac{\pi_\theta(y_n \mid x, m_p)}{\pi_{\text{ref}}(y_n \mid x, m_p)}\Big). \quad (9)$$

Our final loss combines both visual and textual preference signals,

$$\mathcal{L}(\theta; \tilde{\mathcal{S}}_n) = \mathcal{L}_{\text{img}}(\theta; \tilde{\mathcal{S}}_n) + \lambda\, \mathcal{L}_{\text{text}}(\theta; \tilde{\mathcal{S}}_n). \quad (10)$$

where λ balances the contributions of image-based and text-based supervision. This unified formulation supports joint alignment across modalities, improving robustness and alignment quality in VLMs.

4.2 IMPORTANCE SAMPLING VIA SPARSE AUTOENCODER

To address the limitations of existing methods that rely on simplistic, one-dimensional negatives, we employ SAEs to disentangle and surface semantically meaningful variations in the visual space. By providing a structured and interpretable latent representation, SAEs enable principled importance sampling over diverse negative examples—prioritizing those that capture distinct failure modes and are most informative for effective preference learning.

Embedding and Difference Vectors. Let $\mathcal{T} = \{(m_p, x)\}$ be the training set of positive image–prompt pairs. We use CLIP's image and text encoders, f_v and f_t, to obtain d-dimensional embeddings $h_v = f_v(m_p)$ and $h_t = f_t(x)$, then fuse them via outer product and vectorization $e = \text{vec}\big(h_v \times h_t^\top\big) \in \mathbb{R}^{d^2}$. For each negative candidate m_n^i, we form the difference vector

$$d_i \;=\; e(m_p, x) \;-\; e(m_n^i, x).$$

Sparse Autoencoder Training. We train an SAE with encoder $\mathcal{E}$ and decoder $\mathcal{D}$ to decompose d_i into sparse latent factors. The loss combines reconstruction fidelity and activation sparsity,

$$\mathcal{L}_{\text{SAE}} = \frac{1}{|\mathcal{T}|N} \sum_{(m_p,x)\in\mathcal{T}} \sum_{i=1}^{N} \big\| d_i - \mathcal{D}\big(\mathcal{E}(d_i)\big)\big\|_2^2 + \gamma \sum_{j=1}^{H} \text{KL}\big(\rho \| \hat{\rho}_j\big), \quad (11)$$

where$\hat{\rho}_j$ is the average activation of hidden unit j, $\rho \in (0, 1)$ is the target average activation, and γ balances reconstruction against sparsity.

Diverse Negative Selection. We score each candidate m_n^i by,

$$s_i = \frac{\big\|d_i - \mathcal{D}(\mathcal{E}(d_i))\big\|_2^2}{\max_j \ell_j} + \frac{\big\|\mathcal{E}(d_i)\big\|_1}{\max_j v_j}, \quad (12)$$

where ℓ_j and v_j are the reconstruction error and activation magnitude across all candidates. To choose the final top-K negatives $\tilde{\mathcal{S}}_n$, we run a greedy selection that maximizes coverage of distinct error types while emphasizing hard negatives. We illustrate this algorithm in detail in Algorithm 1.

The selected set $\tilde{\mathcal{S}}_n$ is then used in the importance-sampling gradient estimator of Eq. equation 8.

Algorithm 1 Greedy Diversity-Promoting Selection

```
**Input:** Difference vectors $\{d_i\}_{i=1}^N$, scores $\{s_i\}$, encoder $\mathcal{E}$, selection size $K$
$\tilde{\mathcal{S}}_n \leftarrow \emptyset$
**while** $|\tilde{\mathcal{S}}_n| < K$ **do**
    $i^* \leftarrow \arg\max_{i \notin \tilde{\mathcal{S}}_n} \Big( s_i + \beta \, \min_{j \in \tilde{\mathcal{S}}_n} (1 - \cos(\mathcal{E}(d_i), \mathcal{E}(d_j))) \Big)$
    $\tilde{\mathcal{S}}_n \leftarrow \tilde{\mathcal{S}}_n \cup \{i^*\}$
**end while**
**Output:** selected negatives set $\tilde{\mathcal{S}}_n$
```

5 EXPERIMENT

5.1 EXPERIMENTAL SETTINGS

Models. We apply MISP-DPO to three widely-used multimodal LLMs: LLaVA-1.5-7B-HF, Qwen2.5-VL-7B, and Qwen2.5-VL-3B. These models are chosen due to their open availability, competitive performance, and diverse architectural designs (Chen et al., 2024b; Zhang et al., 2024). LLaVA-1.5-7B-HF (Liu et al., 2023) integrates CLIP as the vision encoder with Vicuna-1.5-7B as the language backbone. Qwen2.5-VL-7B (Bai et al., 2025) uses a proprietary vision module and the strong Qwen2.5-7B language model. Qwen2.5-VL-3B is a lightweight 3B variant of the same architecture, providing a better balance between efficiency and capability.

Training data. We choose RLHF-V-Dataset (Yu et al., 2024) as our training dataset. It contains more than 5K samples, each with an image and a pair of text responses indicating preference. RLHF-V provides fine-grained, segment-level human feedback on diverse vision-language instructions, which has been shown to largely reduce hallucination while preserving informativeness. We treat the paired image as the positive sample and select 3 negative images per sample from COCO training dataset (Lin et al., 2014) using our importance sampling method, enabling effective training in our MISP-DPO framework.

Baselines. We compare MISP-DPO against five baselines: (1) the pretrained model without preference tuning, (2) standard DPO (Rafailov et al., 2023), which uses only a single text preference without any image-based supervision, (3) mDPO (Wang et al., 2024a) and (4) CHiP (Fu et al., 2025), both of which incorporate image preferences but rely on a single negative image per comparison, and (5) a variant of our framework that uses multi-negative image preference optimization with negatives randomly sampled from the COCO dataset. All methods are trained under the same settings for a fair comparison.

Evaluation Benchmarks. We evaluate MISP-DPO and all baselines across five benchmarks spanning hallucination detection and vision-centric reasoning. MMHal-Bench(Sun et al., 2023) is a hallucination-focused VQA benchmark covering 8 question types and 12 object categories. HallusionBench(Guan et al., 2024) measures visual and factual hallucinations; we report all-answer accuracy (aA), figure-based accuracy (fA), and question-type accuracy (qA). POPE(Li et al., 2023b) evaluates object hallucination in VLMs via Yes/No probing under random, popular, and adversarial object settings. WildVision(Lu et al., 2024) evaluates real-world user preference alignment with 500 curated human-model interaction samples; we report reward score and win rate. MMVP(Tong et al., 2024) assesses fine-grained visual reasoning using CLIP-blind image pairs, with accuracy reported over 135 zero-shot questions across 9 pattern types. Except for MMHal-Bench, all evaluations are conducted using VLMEvalKit(Duan et al., 2024), an open-source evaluation toolkit for vision-language models. For MMHal-Bench, we use GPT-4.1-mini(Achiam et al., 2023) as the evaluator and report overall response quality and hallucination rate.

Implementation Details. For training the Sparse Autoencoder, we set the latent dimension to 128 and the sparsity weight γ to 1, balancing reconstruction fidelity with latent sparsity. Following prior work on multi-negative preference optimization (Chen et al., 2024a), we select three negative images per instance. For multimodal DPO training, we set the supervision balance parameter λ to 1 to equally weight image-based and text-based preferences. All models are fine-tuned using 2 NVIDIA A100 GPUs, with a per-device batch size of 2, gradient accumulation steps of 8 (yielding an effective batch size of 32), and a learning rate of 10^{-5}. The preference optimization coefficient β

		Hallucination						**Vision-Centric**			**Total**
	Benchmarks	**MMHalBench**		**HallusionBench**			**POPE**	**WildVision**		**MMVP**	**avg_impr.**
		Score (↑)	**HalRate** (↓)	**aA** (↑)	**fA** (↑)	**qA** (↑)	**Acc.** (↑)	**Reward** (↑)	**WinRate** (↑)	**Acc.** (↑)	**over BASE**
llava-1.5-7b-hf	Base	2.78	51.04	47.73	17.63	12.30	**84.37**	-55.7	17.0	60.67	0%
	DPO	3.29	37.50	55.62	22.83	22.63	83.02	-52.7	18.4	62.66	+21.13%
	mDPO	2.99	49.81	47.32	20.52	13.19	83.25	-62.1	14.6	58.33	+0.22%
	CHiP	3.13	34.04	51.95	17.92	19.78	82.56	-68.4	12.2	52.33	+5.59%
	Random	3.42	36.46	55.94	23.69	22.63	82.61	-51.3	18.3	60.33	+22.23%
	MISP-DPO	**3.51**	**32.29**	**57.52**	**25.43**	**24.83**	83.94	**-46.4**	**20.6**	**63.00**	**+30.09%**
Qwen2.5-VL-7B	Base	4.61	18.09	70.45	43.06	45.27	87.65	**33.5**	**69.2**	77.67	0%
	DPO	4.92	**11.46**	69.92	42.48	43.51	87.46	32.8	68.6	78.00	+3.85%
	mDPO	5.01	14.89	67.40	41.33	42.20	87.02	28.5	66.2	76.33	-1.16%
	CHiP	5.02	13.83	66.14	39.02	40.88	88.18	28.5	66.4	77.00	-1.33%
	Random	4.75	16.67	70.24	42.48	43.95	87.60	30.7	67.8	78.33	-0.36%
	MISP-DPO	**5.05**	**11.46**	**71.24**	**43.77**	**45.61**	**88.66**	32.4	68.4	**79.00**	**+5.35%**
Qwen2.5-VL-3B	Base	4.20	22.34	64.67	37.57	36.70	87.48	-0.1	46.6	70.60	0%
	DPO	4.50	18.75	65.19	36.41	37.14	87.42	7.5	51.2	71.33	+13.12%
	mDPO	4.47	21.28	62.88	35.84	37.14	87.65	7.2	50.8	69.33	+10.51%
	CHiP	4.51	15.96	62.14	36.13	34.29	87.30	6.3	51.0	70.33	+11.81%
	Random	4.27	16.67	64.98	**38.44**	37.36	87.52	3.6	48.6	74.25	+8.57%
	MISP-DPO	**4.61**	**13.54**	**65.51**	**38.44**	**38.02**	**87.77**	**8.6**	**52.4**	**72.00**	**+19.89%**

Table 1: Comparison of MISP-DPO against baseline methods across five vision–language benchmarks and three model backbones. The benchmarks cover hallucination detection and vision-centric reasoning. Average improvement over BASE is reported. ↑: higher is better; ↓: lower is better.

is set to 0.5. Following prior work on mDPO, we adopt LoRA for parameter-efficient tuning, with a rank of 64 and scaling factor $\alpha = 128$. For baseline methods, we strictly follow their original settings: mDPO is trained for 3 epochs with the same learning rate (1e-5), $\beta = 0.1$; CHiP is trained for 3 epochs with a batch size of 32, a learning rate of 5e-7, $\beta = 0.5$, and full-parameter finetuning.

5.2 OVERALL PERFORMANCE IMPROVEMENT

Table 1 shows the performance of MISP-DPO and baselines across five representative benchmarks, grouped into two categories: hallucination detection (MMHalBench, HallusionBench, POPE) and vision-centric reasoning (WildVision, MMVP). Our proposed MISP-DPO consistently achieves superior results over all evaluation domains and model backbones.

The largest gains appear on hallucination benchmarks. MISP-DPO substantially reduces hallucination rates on MMHalBench (e.g., 32.29%, 11.46%, and 13.54% across different backbones) while also achieving the highest accuracy across all HallusionBench metrics. POPE further confirms these advantages. These improvements stem from the combination of diverse negative sampling, which exposes the model to varied error types such as object mismatches and attribute distortions, and importance sampling, which prioritizes hard negatives with high reconstruction errors from SAE, leading to stronger visual grounding. On vision-centric reasoning tasks, MISP-DPO also provides consistent gains. For example, it achieves the best reward (+8.6) and win rate (52.4) on WildVision for Qwen2.5-VL-3B, while also outperforming baselines on MMVP across different model sizes. These results suggest that our method not only suppresses hallucinations but also enhances the model's ability to generate fine-grained, visually aligned responses.

We also conduct experiments under different β values on MMHalBench to balance reward learning and regularization. Figure 4 reveals performance peaks at β ranging from 0.45 to 0.75, with degradation at extremes $\beta = 0.1/1.0$. We choose $\beta = 0.5$ for optimal trade-off between hallucination control and response quality, as it maximizes accuracy while minimizing hallucination rates across all backbones.

5.3 EFFECTIVENESS OF IMPORTANCE SAMPLING

We analyze the impact of our importance sampling strategy using t-SNE visualizations of high-quality negative images, shown in Figure 2. The left plot displays negatives selected by our SAE-guided strategy, while the middle shows randomly sampled ones. Importance-sampled negatives

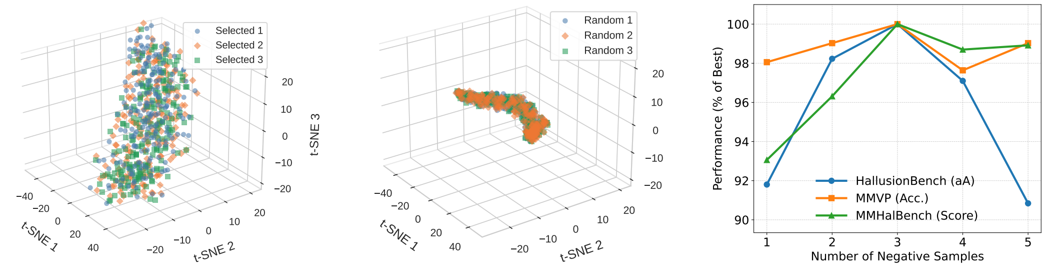

Figure 2: t-SNE visualizations and benchmark results for negative sampling. **Left:** importance-sampled negatives selected using SAE scoring exhibit broad semantic dispersion across three selections. **Middle:** randomly sampled negatives form tight, low-diversity clusters. **Right:** performance across benchmarks with different numbers of negatives selected by MISP-DPO.

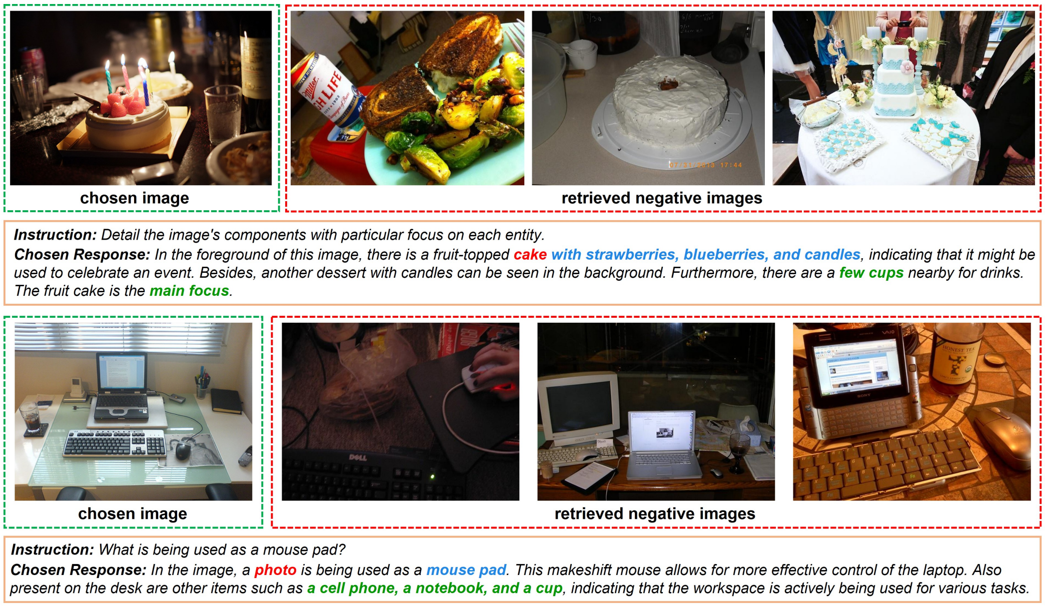

Instruction: *Detail the image's components with particular focus on each entity.*
Chosen Response: *In the foreground of this image, there is a fruit-topped* ***cake*** ***with strawberries, blueberries, and candles****, indicating that it might be used to celebrate an event. Besides, another dessert with candles can be seen in the background. Furthermore, there are a* ***few cups*** *nearby for drinks. The fruit cake is the* ***main focus****.*

Instruction: *What is being used as a mouse pad?*
Chosen Response: *In the image, a* ***photo*** *is being used as a* ***mouse pad****. This makeshift mouse allows for more effective control of the laptop. Also present on the desk are other items such as* ***a cell phone, a notebook, and a cup****, indicating that the workspace is actively being used for various tasks.*

Figure 3: Negative image retrieval using our MISP-DPO method. Each row shows a chosen image and three negatives; highlighted phrases in **red**, **blue** and **green** mark mismatches with negatives.

are well-dispersed across the embedding space, indicating high semantic diversity, whereas random negatives cluster tightly, indicating redundancy and limited coverage. This distribution reveals that our method captures heterogeneous error modes rather than collapsing onto a narrow, repetitive subset of examples, thereby providing more informative supervision.

As illustrated in Figure 3, our selected negatives for the fruit cake image exhibit clear semantic deviations: one introduces different types of cakes with distinct decorations, while others include unrelated food items such as sandwiches, or scenes where the cake is present but not the main visual focus, thereby weakening semantic alignment. Similarly, in the workspace scene, negative examples capture meaningful variations such as differences in desk arrangement and surrounding objects—including notebooks and cups—each impacting multimodal alignment differently. These examples highlight how our sampling method uncovers diverse error modes, encouraging the model to learn more robust visual distinctions, strengthening training signals, and improving generalization beyond narrow, one-dimensional deviations.

5.4 COMPARISON OF NEGATIVE SAMPLING STRATEGIES

We evaluate five negative sampling strategies that share the same model architecture and loss formulation but differ in how negative images are constructed: (1) mDPO, which relies on a single diffusion-generated negative; (2) diffusion, which combines one diffusion negative with two negatives selected by our method; (3) crop+diffusion, which mixes one cropped, one diffusion, and

Model	**Benchmark**	**MMHalBench**		**HallusionBench**			**POPE**	**WildVision**		**MMVP**
		Score (↑)	**HalRate (↓)**	**aA (↑)**	**fA (↑)**	**qA (↑)**	**Acc. (↑)**	**Reward (↑)**	**WinRate (↑)**	**Acc. (↑)**
Qwen2.5-7B	mdpo	5.01	14.89	67.40	41.33	42.20	87.02	28.5	66.2	76.33
	diffusion	**5.12**	12.50	69.50	43.64	43.95	87.52	30.7	66.4	78.00
	crop+diffusion	4.92	13.54	70.35	43.35	44.61	87.35	30.7	66.4	78.33
	similarity	5.00	12.50	69.82	42.77	44.17	87.24	30.1	66.2	77.67
	MISP-DPO	5.05	**11.46**	**71.24**	**43.77**	**45.61**	**88.66**	**32.4**	**68.4**	**79.00**
Qwen2.5-3B	mDPO	4.47	21.28	62.88	35.84	37.14	87.65	7.2	50.8	69.33
	diffusion	4.56	14.58	65.19	**39.31**	37.14	87.35	8.0	**52.4**	71.33
	crop+diffusion	4.39	17.70	64.03	38.44	36.48	87.20	5.3	49.8	71.33
	similarity	4.20	19.79	65.08	39.01	36.92	87.62	4.7	49.4	70.30
	MISP-DPO	**4.61**	**13.54**	**65.51**	38.44	**38.02**	**87.77**	**8.6**	**52.4**	**72.00**

Table 2: Comparison of different negative sampling strategies across five benchmarks. All variants share the same model and loss design, differing only in how negative images are constructed.

one MISP-DPO-selected negative; (4) similarity, where three negatives are retrieved based on similarity to the positive image; and (5) our model. As shown in Table 2, mDPO yields the weakest performance, highlighting the limitations of single-negative supervision. Among multi-negative variants, the diffusion strategy outperforms crop+diffusion, suggesting that a higher proportion of semantically diverse negatives from our method improves supervision quality. The similarity variant performs worse than diffusion, underscoring that naive retrieval of visually similar negatives does not provide the challenging guidance needed. In contrast, MISP-DPO consistently achieves the best scores across all benchmarks, validating the effectiveness of structured multi-negative selection via SAE-guided importance sampling. Additional results are reported in Table 3 in the appendix.

Beyond the choice of sampling strategy, we further explore the number of negatives required. Figure 2 (right) shows performance across HallusionBench, MMVP, and MMHalBench with varying numbers of negatives. One or two negatives are insufficient to provide high-quality supervision. Performance peaks at three negatives, while increasing beyond this offers no further benefit. For HallusionBench, adding five negatives even reduces performance, likely due to noise introduced by redundant or low-quality samples. Together, these results demonstrate that three carefully chosen negatives strike the best balance between informativeness and robustness.

5.5 HALLUCINATION REDUCTION WITH MISP-DPO.

Figure 5 in the Appendix presents qualitative comparisons highlighting the impact of multi-negative supervision. Baseline methods such as DPO and CHiP frequently introduce hallucinated details (e.g., incorrect objects, colors, or spatial relations), while MISP-DPO generates more faithful and grounded descriptions. For instance, in the first example, only MISP-DPO correctly identifies that the image lacks sand and accurately describes the bird. These results illustrate that incorporating diverse negatives enables the model to better distinguish relevant from spurious cues, improving factual accuracy in vision-language alignment.

6 CONCLUSION

We present MISP-DPO, a novel framework that introduces multi-negative, semantically diverse supervision into multimodal Direct Preference Optimization. By leveraging CLIP-based embeddings and a sparse autoencoder, our method efficiently selects image-side negatives that vary across multiple semantic facets and reflect diverse failure modes. These negatives are integrated into a Plackett-Luce-style ranking objective with importance sampling, enabling the model to learn from richer and more structured supervision. The method remains efficient and scalable for real-world multimodal applications. Extensive experiments across five benchmarks demonstrate that MISP-DPO consistently outperforms strong baselines in hallucination reduction and visual grounding. While our evaluations rely on GPT-based scoring—which may introduce bias or inconsistency when assessing fine-grained alignment—our findings validate the effectiveness of semantic-aware, multi-negative sampling for robust multimodal alignment and open up promising directions for scalable and interpretable preference-based learning.

REFERENCES

Josh Achiam, Steven Adler, Sandhini Agarwal, Lama Ahmad, Ilge Akkaya, Florencia Leoni Aleman, Diogo Almeida, Janko Altenschmidt, Sam Altman, Shyamal Anadkat, et al. Gpt-4 technical report. *arXiv preprint arXiv:2303.08774*, 2023.

Afra Amini, Tim Vieira, and Ryan Cotterell. Direct preference optimization with an offset. *arXiv preprint arXiv:2402.10571*, 2024.

Shuai Bai, Keqin Chen, Xuejing Liu, Jialin Wang, Wenbin Ge, Sibo Song, Kai Dang, Peng Wang, Shijie Wang, Jun Tang, et al. Qwen2. 5-vl technical report. *arXiv preprint arXiv:2502.13923*, 2025.

Lior Baruch, Moshe Butman, Kfir Bar, and Doron Friedman. Preference tree optimization: Enhancing goal-oriented dialogue with look-ahead simulations. In *Scaling Self-Improving Foundation Models without Human Supervision*.

Yuxin Chen, Junfei Tan, An Zhang, Zhengyi Yang, Leheng Sheng, Enzhi Zhang, Xiang Wang, and Tat-Seng Chua. On softmax direct preference optimization for recommendation. *arXiv preprint arXiv:2406.09215*, 2024a.

Zhe Chen, Weiyun Wang, Yue Cao, Yangzhou Liu, Zhangwei Gao, Erfei Cui, Jinguo Zhu, Shenglong Ye, Hao Tian, Zhaoyang Liu, et al. Expanding performance boundaries of open-source multimodal models with model, data, and test-time scaling. *arXiv preprint arXiv:2412.05271*, 2024b.

Yihe Deng, Pan Lu, Fan Yin, Ziniu Hu, Sheng Shen, Quanquan Gu, James Y Zou, Kai-Wei Chang, and Wei Wang. Enhancing large vision language models with self-training on image comprehension. *Advances in Neural Information Processing Systems*, 37:131369–131397, 2024.

Haodong Duan, Junming Yang, Yuxuan Qiao, Xinyu Fang, Lin Chen, Yuan Liu, Xiaoyi Dong, Yuhang Zang, Pan Zhang, Jiaqi Wang, et al. Vlmevalkit: An open-source toolkit for evaluating large multi-modality models. In *Proceedings of the 32nd ACM international conference on multimedia*, pp. 11198–11201, 2024.

Jinlan Fu, Shenzhen Huangfu, Hao Fei, Xiaoyu Shen, Bryan Hooi, Xipeng Qiu, and See-Kiong Ng. Chip: Cross-modal hierarchical direct preference optimization for multimodal llms. *arXiv preprint arXiv:2501.16629*, 2025.

Tianrui Guan, Fuxiao Liu, Xiyang Wu, Ruiqi Xian, Zongxia Li, Xiaoyu Liu, Xijun Wang, Lichang Chen, Furong Huang, Yaser Yacoob, et al. Hallusionbench: an advanced diagnostic suite for entangled language hallucination and visual illusion in large vision-language models. In *Proceedings of the IEEE/CVF Conference on Computer Vision and Pattern Recognition*, pp. 14375–14385, 2024.

Cheng-Yu Hsieh, Jieyu Zhang, Zixian Ma, Aniruddha Kembhavi, and Ranjay Krishna. Sugarcrepe: Fixing hackable benchmarks for vision-language compositionality. *Advances in neural information processing systems*, 36:31096–31116, 2023.

Songtao Jiang, Yan Zhang, Ruizhe Chen, Yeying Jin, and Zuozhu Liu. Modality-fair preference optimization for trustworthy mllm alignment. *arXiv preprint arXiv:2410.15334*, 2024.

Amita Kamath, Jack Hessel, and Kai-Wei Chang. Text encoders bottleneck compositionality in contrastive vision-language models. *arXiv preprint arXiv:2305.14897*, 2023.

Amita Kamath, Cheng-Yu Hsieh, Kai-Wei Chang, and Ranjay Krishna. The hard positive truth about vision-language compositionality. In *European Conference on Computer Vision*, pp. 37–54. Springer, 2024.

Bohao Li, Rui Wang, Guangzhi Wang, Yuying Ge, Yixiao Ge, and Ying Shan. Seed-bench: Benchmarking multimodal llms with generative comprehension. *arXiv preprint arXiv:2307.16125*, 2023a.

Yifan Li, Yifan Du, Kun Zhou, Jinpeng Wang, Wayne Xin Zhao, and Ji-Rong Wen. Evaluating object hallucination in large vision-language models. *arXiv preprint arXiv:2305.10355*, 2023b.

Tsung-Yi Lin, Michael Maire, Serge Belongie, James Hays, Pietro Perona, Deva Ramanan, Piotr Dollár, and C Lawrence Zitnick. Microsoft coco: Common objects in context. In *Computer vision–ECCV 2014: 13th European conference, zurich, Switzerland, September 6-12, 2014, proceedings, part v 13*, pp. 740–755. Springer, 2014.

Chaohu Liu, Tianyi Gui, Yu Liu, and Linli Xu. Adpo: Enhancing the adversarial robustness of large vision-language models with preference optimization. *arXiv preprint arXiv:2504.01735*, 2025.

Haotian Liu, Chunyuan Li, Qingyang Wu, and Yong Jae Lee. Visual instruction tuning. *Advances in neural information processing systems*, 36:34892–34916, 2023.

Yujie Lu, Dongfu Jiang, Wenhu Chen, William Yang Wang, Yejin Choi, and Bill Yuchen Lin. Wildvision: Evaluating vision-language models in the wild with human preferences. *arXiv preprint arXiv:2406.11069*, 2024.

R Duncan Luce et al. *Individual choice behavior*, volume 4. Wiley New York, 1959.

Robin L Plackett. The analysis of permutations. *Journal of the Royal Statistical Society Series C: Applied Statistics*, 24(2):193–202, 1975.

Alec Radford, Jong Wook Kim, Chris Hallacy, Aditya Ramesh, Gabriel Goh, Sandhini Agarwal, Girish Sastry, Amanda Askell, Pamela Mishkin, Jack Clark, et al. Learning transferable visual models from natural language supervision. In *International conference on machine learning*, pp. 8748–8763. PmLR, 2021.

Rafael Rafailov, Archit Sharma, Eric Mitchell, Christopher D Manning, Stefano Ermon, and Chelsea Finn. Direct preference optimization: Your language model is secretly a reward model. *Advances in Neural Information Processing Systems*, 36:53728–53741, 2023.

Ugur Sahin, Hang Li, Qadeer Khan, Daniel Cremers, and Volker Tresp. Enhancing multimodal compositional reasoning of visual language models with generative negative mining. In *Proceedings of the IEEE/CVF Winter Conference on Applications of Computer Vision*, pp. 5563–5573, 2024.

Wentao Shi, Mengqi Yuan, Junkang Wu, Qifan Wang, and Fuli Feng. Direct multi-turn preference optimization for language agents. *arXiv preprint arXiv:2406.14868*, 2024.

Zhiqing Sun, Sheng Shen, Shengcao Cao, Haotian Liu, Chunyuan Li, Yikang Shen, Chuang Gan, Liang-Yan Gui, Yu-Xiong Wang, Yiming Yang, et al. Aligning large multimodal models with factually augmented rlhf. *arXiv preprint arXiv:2309.14525*, 2023.

Shengbang Tong, Zhuang Liu, Yuexiang Zhai, Yi Ma, Yann LeCun, and Saining Xie. Eyes wide shut? exploring the visual shortcomings of multimodal llms. In *Proceedings of the IEEE/CVF Conference on Computer Vision and Pattern Recognition*, pp. 9568–9578, 2024.

Fei Wang, Wenxuan Zhou, James Y Huang, Nan Xu, Sheng Zhang, Hoifung Poon, and Muhao Chen. mdpo: Conditional preference optimization for multimodal large language models. *arXiv preprint arXiv:2406.11839*, 2024a.

Xin Wang, Hong Chen, Si'ao Tang, Zihao Wu, and Wenwu Zhu. Disentangled representation learning. *IEEE Transactions on Pattern Analysis and Machine Intelligence*, 2024b.

Shengguang Wu, Fan-Yun Sun, Kaiyue Wen, and Nick Haber. Symmetrical visual contrastive optimization: Aligning vision-language models with minimal contrastive images. *arXiv preprint arXiv:2502.13928*, 2025.

Shuo Xing, Yuping Wang, Peiran Li, Ruizheng Bai, Yueqi Wang, Chengxuan Qian, Huaxiu Yao, and Zhengzhong Tu. Re-align: Aligning vision language models via retrieval-augmented direct preference optimization. *arXiv preprint arXiv:2502.13146*, 2025.

An Yan, Yu Wang, Yiwu Zhong, Chengyu Dong, Zexue He, Yujie Lu, William Yang Wang, Jingbo Shang, and Julian McAuley. Learning concise and descriptive attributes for visual recognition. In *Proceedings of the IEEE/CVF International Conference on Computer Vision*, pp. 3090–3100, 2023.

Tianyu Yu, Yuan Yao, Haoye Zhang, Taiwen He, Yifeng Han, Ganqu Cui, Jinyi Hu, Zhiyuan Liu, Hai-Tao Zheng, Maosong Sun, et al. Rlhf-v: Towards trustworthy mllms via behavior alignment from fine-grained correctional human feedback. In *Proceedings of the IEEE/CVF Conference on Computer Vision and Pattern Recognition*, pp. 13807–13816, 2024.

Yunan Zeng, Yan Huang, Jinjin Zhang, Zequn Jie, Zhenhua Chai, and Liang Wang. Investigating compositional challenges in vision-language models for visual grounding. In *Proceedings of the IEEE/CVF Conference on Computer Vision and Pattern Recognition*, pp. 14141–14151, 2024.

Duzhen Zhang, Yahan Yu, Jiahua Dong, Chenxing Li, Dan Su, Chenhui Chu, and Dong Yu. Mm-llms: Recent advances in multimodal large language models. *arXiv preprint arXiv:2401.13601*, 2024.

Chenhao Zheng, Jieyu Zhang, Aniruddha Kembhavi, and Ranjay Krishna. Iterated learning improves compositionality in large vision-language models. In *Proceedings of the IEEE/CVF Conference on Computer Vision and Pattern Recognition*, pp. 13785–13795, 2024.

A APPENDIX

A.1 EFFECT OF β ON HALLUCINATION AND QUALITY

Figure 4 illustrates the impact of different β values on both response quality (left) and hallucination rate (right) on MMHalBench. We observe that the model performs best when β lies in the range of 0.45 to 0.75, achieving a good balance between response quality and hallucination suppression. To ensure both accuracy and stability, we set $\beta = 0.5$ as the default value in all main experiments.

A.2 EXAMPLES OF HALLUCINATION REDUCTION WITH MISP-DPO

To illustrate the impact of our approach, Figure 5 presents qualitative comparisons across three representative prompts, highlighting the improvements brought by MISP-DPO over baselines including LLaVA, DPO, and CHiP. MISP-DPO demonstrates a stronger ability to avoid hallucinations and produce factually accurate descriptions grounded in visual evidence. In the first example, it correctly identifies the absence of sand and avoids misidentifying the bird species. In the second case, it faithfully describes the structure and positioning of the gloves despite occlusion. In the final example, it provides a precise spatial interpretation of the two watches without fabricating brand-specific details. These results suggest that our multi-negative supervision strategy improves the model's sensitivity to fine-grained semantic cues and its ability to reject spurious correlations and hallucinated attributes, leading to more factually consistent vision-language generation.

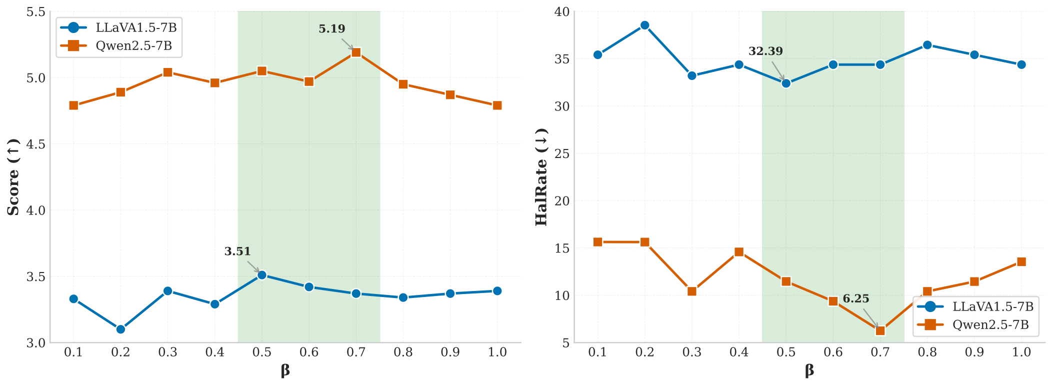

Figure 4: Performance comparison of Score and Hallucination Rate across different β values for on MMHalBench.

A.3 UNBIASEDNESS AND FINITE-SAMPLE VARIANCE BOUNDS FOR IMPORTANCE SAMPLING GRADIENT

For convenience, we define the inner gradient term in Lemma 4.1,

$$g(\theta) := \sum_{i=1}^{N} p_\theta(m_n^i \mid x, m_p, y_p)\, \Delta_\theta(m_n^i, m_p \mid x, y_p). \tag{13}$$

Our importance-sampling scheme (Sec. 4.1) introduces a proposal distribution $q_\phi(m_n \mid x, m_p, y_p)$ induced by the CLIP+SAE pipeline, and samples a small candidate pool $\widetilde{\mathcal{S}}_n = \{m_n^k\}_{k=1}^K$ from q_ϕ. We then approximate the exact gradient using an importance-weighted estimator.

A.3.1 UNBIASEDNESS OF THE IS GRADIENT

Let the importance weight be

$$w(m_n) = \frac{p_\theta(m_n \mid x, m_p, y_p)}{q_\phi(m_n \mid x, m_p, y_p)}.$$

Lemma A.1 (Unbiased IS gradient) *Assume that* $q_\phi(m_n \mid x, m_p, y_p) > 0$ *whenever* $p_\theta(m_n \mid x, m_p, y_p) > 0$*. Define the Monte Carlo estimator of* $g(\theta)$ *as,*

$$\widehat{g}_k(\theta) := \frac{1}{K} \sum_{k=1}^{K} w\big(m_n^k\big)\ \Delta_\theta\big(m_n^k, m_p \mid x, y_p\big), \quad m_n^k \sim q_\phi(\cdot \mid x, m_p, y_p).$$

Then $\hat{g}_k(\theta)$ *is an unbiased estimator of* $g(\theta)$*,*

$$\mathbb{E}_{\{m_n^k\}\sim q_\phi}\big[\widehat{g}_k(\theta)\big] = g(\theta). \tag{14}$$

Proof A.1 *Using linearity of expectation and the definition of importance weights,*

$$\begin{aligned}
\mathbb{E}_{\{m_n^k\}\sim q_\phi}\big[\widehat{g}_k(\theta)\big] &= \mathbb{E}_{m\sim q_\phi}\big[w(m_n)\,\Delta_\theta(m_n, m_p \mid x, y_p)\big] \\
&= \sum_{i=1}^{N} q_\phi(m_n^i \mid x, m_p, y_p)\,\frac{p_\theta(m_n^i \mid x, m_p, y_p)}{q_\phi(m_n^i \mid x, m_p, y_p)}\,\Delta_\theta(m_n^i, m_p \mid x, y_p) \\
&= \sum_{i=1}^{N} p_\theta(m_n^i \mid x, m_p, y_p)\,\Delta_\theta(m_n^i, m_p \mid x, y_p) \\
&= g(\theta),
\end{aligned}$$

which proves the claim.

Thus, the IS estimator recovers the exact gradient term in expectation, and hence the overall gradient in Eq. 7,

$$\nabla_\theta L_{\mathrm{img}}(\theta; \mathcal{S}_n) = \beta\,\sigma\Big(\log \sum_{i=1}^{N} \exp(a_i)\Big) g(\theta), \tag{15}$$

admits an unbiased importance-sampling estimator by replacing $g(\theta)$ with $\widehat{g}_k(\theta)$.

A.3.2 VARIANCE BOUND UNDER FINITE NEGATIVE SAMPLING

We next calculate the variance of $\widehat{g}_k(\theta)$ when only a finite number K of negatives are sampled.

Define the maximum importance weight,

$$\|w\|_\infty := \max_{m_n \in \mathcal{S}_n} \frac{p_\theta(m_n \mid x, m_p, y_p)}{q_\phi(m_n \mid x, m_p, y_p)}.$$

Assume that the gradient differences are bounded, which in practice is achieved by gradient clipping [4-6]. There exists $L < \infty$ such that,

$$\big\|\Delta_\theta(m_n, m_p \mid x, y_p)\big\|_2 \le L \quad \forall m_n \in \mathcal{S}_n. \tag{16}$$

Lemma A.2 (Variance bound) *Under the assumptions above, the mean-square error of the IS gradient estimator isbounded as,*

$$\mathbb{E}\big[\|\widehat{g}_k(\theta) - g(\theta)\|_2^2\big] \ \le\ \frac{L^2}{K}\,\|w\|_\infty.$$

Consequently, the expected absolute deviation satisfies,

$$\mathbb{E}\big[\|\widehat{g}_k(\theta) - g(\theta)\|_2\big] \ \le\ L\sqrt{\frac{\|w\|_\infty}{K}}. \tag{17}$$

Proof A.2 *Because the* K *samples are i.i.d.,*

$$\mathrm{Var}\big(\widehat{g}_k(\theta)\big) = \frac{1}{K}\,\mathrm{Var}\big(w(m_n)\Delta_\theta(m_n, m_p \mid x, y_p)\big).$$

Using the bound $\left\|\Delta_\theta(m_n, m_p \mid x, y_p)\right\|_2 \le L$, *we obtain*

$$\begin{aligned}
\mathbb{E}\big[\|\widehat{g}_k(\theta) - g(\theta)\|_2^2\big] &\le \frac{1}{K}\,\mathbb{E}_{m_n\sim q_\phi}\big[\|w(m_n)\Delta_\theta(m_n, m_p \mid x, y_p)\|_2^2\big] \\
&\le \frac{L^2}{K}\,\mathbb{E}_{m_n\sim q_\phi}\big[w(m_n)^2\big].
\end{aligned}$$

Moreover,

$$\begin{aligned}
\mathbb{E}_{m_n\sim q_\phi}\big[w(m_n)^2\big] &\le \|w\|_\infty\,\mathbb{E}_{m\sim q_\phi}[w(m_n)] \\
&= \|w\|_\infty \sum_{m_n} q_\phi(m_n)\,\frac{p_\theta(m_n)}{q_\phi(m_n)} = \|w\|_\infty \sum_{m_n} p_\theta(m_n) = \|w\|_\infty .
\end{aligned} \tag{18}$$

Combining these yields the desired variance bound. Applying Cauchy–Schwarz gives the final variance bound.

In our setting, the SAE-guided sampler is explicitly designed to approximate the target distribution with diverse but not overly peaky weights, which empirically keeps $\|w\|_\infty$ small and leads to stable optimization.

A.4 NEGATIVE SAMPLING STRATEGIES ON LLAVA-1.5-7B MODEL

Table 3 shows that LLaVA-1.5-7B follows the same trend as Qwen2.5. The single-negative baseline (mDPO) performs the weakest, while adding more negatives through diffusion or crop+diffusion gives only moderate improvements.

In contrast, MISP-DPO consistently achieves the best results, notably lowering hallucination rate and improving accuracy across HallusionBench, POPE, WildVision, and MMVP. This confirms that our SAE-guided multi-negative sampling generalizes across model families, providing stronger guidance even for smaller-scale vision–language models.

Model	**Benchmark**	**MMHalBench**		**HallusionBench**			**POPE**	**WildVision**		**MMVP**
		Score (↑)	**HalRate** (↓)	**aA** (↑)	**fA** (↑)	**qA** (↑)	**Acc.** (↑)	**Reward** (↑)	**WinRate** (↑)	**Acc.** (↑)
llava-1.5-7b	mDPO	2.99	49.81	47.32	20.52	13.19	83.25	-62.1	14.6	58.33
	diffusion	3.49	33.33	52.57	21.38	18.02	83.25	–53.0	18.8	61.33
	crop+diffusion	3.44	35.42	53.63	22.54	19.78	83.80	-50.5	20.0	61.00
	MISP-DPO	**3.51**	**32.29**	**57.52**	**25.43**	**24.83**	**83.94**	**-46.4**	**20.6**	**63.00**

Table 3: llava performance

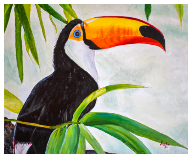

What is a vicuna standing in the sand looking at?

LLaVA	A vicuna standing in the sand is looking at a painting of a bird.
DPO	A vicuna standing in the sand is not looking at anything. In the image, a black and white bird with a yellow and red beak is standing in front of a green leafy plant. The bird is not looking at the plant, but rather at the viewer.
CHiP	A vicuna standing in the sand is looking at a painting of a bird.
MISP-DPO (Ours)	In the image, there is no sand or any other background visible. The painting features a colorful bird with a large beak. It is a black and white bird with a yellow beak, not a vicuna. The bird is surrounded by green and black brush, and the painting is described as a painting of a bird with a yellow beak. The bird is not standing in the sand, and the image does not provide any context or information about the bird looking at something.

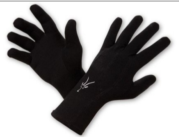

Describe the hands wearing the gloves.

LLaVA	The hands wearing the gloves are large, and the gloves are black in color.
DPO	The hands wearing the gloves are black and have a logo on the palm. The gloves are made of a black material, and the hands are positioned in a way that they are facing upwards.
CHiP	In the image, the hands wearing the gloves are black in color.
MISP-DPO (Ours)	The image shows two black gloves, one of which has a logo on the back. They are positioned in such a way that they appear to be two hands. The gloves are black and have a close-up view, making it difficult to discern any other details. The gloves are not attached to any hands, but they are positioned in a way that they appear to be hands.

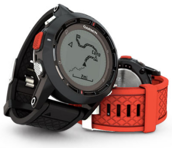

Describe how the two watches are placed.

LLaVA	In the image, there are two watches placed next to each other. One watch is positioned on top of the other, with the top watch being a G-Shock watch and the bottom watch being a Garmin watch. The two watches are placed side by side, showcasing their differences in design and features.
DPO	The watch with the red band is positioned on top of the watch with the black band.The watch with the red band is on the left side of the image, while the watch with the black band is on the left side of the image as well.
CHiP	In the image, one watch is in the foreground, and the other is in the background. The foreground one is a close-up while the other is blurry.
MISP-DPO (Ours)	The two watches are placed side by side, with the Garmin watch on the left and the other watch on the right. The Garmin watch has a screen displaying a map, while the other watch has a red band. The two watches are positioned in such a way that the Garmin watch's screen is visible, and the other watch's red band is also visible.

Figure 5: Comparison of responses from LLaVA model training through different methods: pre-trained, DPO, CHiP, and MISP-DPO. Blue text indicates faithful descriptions; red text marks hallucinated or unsupported content.